ELSEVIER

Physica C 363 (2001) 119–129

PHYSICA C

www.elsevier.com/locate/physc

Superconducting $YBa_2Cu_3O_7$ films grown on TiO_2 buffer layers derived from various processes

K.H. Wu [a,*], P.I. Lin [a], C.C. Hsieh [a], S.J. Liu [a], J.Y. Juang [a], T.M. Uen [a], J.-Y. Lin [b], Y.S. Gou [a]

[a] *Department of Electrophysics, National Chiao Tung University, 1001 Ta Hsueh Road, Hsinchu 30050, Taiwan, ROC*
[b] *Institute of Physics, National Chiao Tung University, 1001 Ta Hsueh Road, Hsinchu 30050, Taiwan, ROC*

Received 27 February 2001; received in revised form 16 April 2001; accepted 16 April 2001

Abstract

$YBa_2Cu_3O_7$ (YBCO)/TiN and YBCO/TiO_2 bilayer structures have been prepared on $SrTiO_3$ (STO)(1 0 0) substrates by in situ pulsed laser deposition (PLD). The TiN films were originally intended to serve as the lower contact electrode for studying the *c*-axis transport properties of YBCO thin films. It was found that, under the optimum conditions of depositing YBCO thin films, the TiN(1 0 0) layer was oxidized and transformed into rutile TiO_2(1 1 0) film. On the other hand, pure anatase TiO_2(0 0 1) films were prepared by PLD using a rutile TiO_2(1 1 0) substrate as the target. YBCO films grown on both phases of TiO_2 films show virtually the same transport properties of typical good quality single-layer YBCO films. Comparative studies of depositing YBCO films directly onto a dc-sputtered TiO_2 template commonly used in the selective epitaxial growth process have, however, resulted in formation of a nonsuperconducting YBCO top layer. Experiments including interfacial X-ray absorption spectroscopy for determining the possible interactions occurring at the YBCO and TiO_2 interface are reported.

PACS: 68.35.Ct; 61.10.Ht; 74.76.Bz; 81.15.Fg
Keywords: TiN films; TiO_2 films; Oxidation of TiN; Pulsed laser deposition; YBCO/TiO_2/STO bilayer structure; Selective epitaxial growth technique; X-ray absorption spectroscopy

1. Introduction

TiN thin films have been studied and used extensively in recent years due to their superior mechanical, thermal, and electrical properties. The widespread applications of TiN films include: (a) hard coatings for high-speed tools, (b) diffusion barriers in microelectronic devices, (c) gold-colored surfaces for cosmetic materials, and (d) transparent conductive films for solar cells or flat panel displays [1–5]. Moreover, it has been suggested that TiN thin films can not only serve as buffer layers in depositing superconducting $YBa_2Cu_3O_7$ (YBCO) thin films on various substrates such as Si, Hastelloy, Inconel and stainless steel, but also as the electrode for metallization and integration of superconductor and semiconductor devices [6,7]. In the light of these peculiar properties exhibited by the TiN films, we have tried to prepare the YBCO/TiN/substrate structure by sequential in situ pulsed laser deposition (PLD) to

* Corresponding author. Tel.: +886-3-5712121, ext. 56114; fax: +886-3-5725230.
E-mail address: khwu@cc.nctu.edu.tw (K.H. Wu).

0921-4534/01/$ - see front matter
PII: S0921-4534(01)00629-3

investigate the out-of-plate (along *c*-axis) transport properties of YBCO thin films. To our surprise, it turned out that such an idea was hindered by the oxidation of TiN layer during the deposition of YBCO thin films. The reaction of TiN films with oxygen is thermodynamically favorable, leading to a significant oxidation rate at temperatures above 400°C [8–11]. Insulating and transparent TiO_2 films with rutile structure were formed following the reaction: $2TiN + 2O_2 \rightarrow 2TiO_2 + N_2$ at temperatures higher than 700°C. Therefore, the originally considered YBCO/TiN/substrate bilayer structure should actually become an YBCO/TiO_2/substrate structure.

Then it is interesting to ask if it makes any difference when the TiO_2 film was obtained directly from a TiO_2 target by PLD. It was found that, under most deposition conditions, pure anatase TiO_2(0 0 l) films were formed even when a pure rutile TiO_2(1 1 0) substrate was used as the target. This result is quite different from those reported previously [12–14], where pure phase and highly oriented TiO_2 films were obtained only under certain deposition conditions. High quality YBCO films also could be obtained with the YBCO/anatase TiO_2(0 0 l)/$SrTiO_3$ (STO)(1 0 0) bilayer structure. It seems reasonable to conclude at this point that, the TiO_2 films can generally serve as excellent buffer layers for growing YBCO films on some technologically important substrates such as Si, sapphire and metallic substrates.

There, however, exist some apparent discrepancies between this conclusion and the results demonstrated in the recently developed selective epitaxial growth (SEG) process [15,16]. The SEG technique is based on the fact that growth of high-quality YBCO films is strongly dependent on structural properties and the morphology of the substrates. Damen et al. [15] and Cheng et al. [16] have used the patterned Ti-template for selective epitaxial growth of micron-sized YBCO structures. As was anticipated, the Ti layer oxidized into TiO_2 prior to the deposition of YBCO thin films. The YBCO thin film grown on the regions covered by the TiO_2 layer became amorphous and exhibited insulating characteristics, while those deposited directly on bare STO substrate regions showed excellent superconductivity. Recently, Chuang et al. [17] have further prepared amorphous TiO_2 layers by dc sputtering and turned it into the selective masked template on a bicrystal STO substrate to in situ fabricate dc SQUID. Again, the TiO_2 layer exhibited excellent selectivity for growing nonsuperconducting YBCO films. In order to resolve these apparent inconsistencies, the crystallinity, surface morphology, interface, and electronic structure of various forms of TiO_2 films have to be examined.

In the present work, we shall report the deposition conditions and the properties of TiN and TiO_2 films prepared by PLD and dc sputtering. The electrical and microstructural properties of YBCO films grown on various TiO_2 templates will be presented. The evidence of the transformation of TiN to TiO_2 during subsequent YBCO deposition will also be shown and discussed. Finally, the differences in surface morphology and X-ray absorption spectroscopy (XAS) measurements are proposed as the primary reasons for apparent inconsistency of the YBCO/TiO_2/substrate obtained by using TiO_2 films prepared by different deposition processes.

2. Experimental details

The PLD system used for preparing the TiN, TiO_2 and YBCO films is the same as that reported previously [18]. Briefly, a KrF excimer laser operating at a repetition rate of 3–8 Hz with an energy density of 2–5 J/cm^2 was used. In order to prepare the bilayer structure in situ, both YBCO and TiN (or TiO_2) targets were installed on a multiple target holder, which was then rotated to bring the desired target in line for ablation. The substrate temperature (T_s) was monitored by a thermocouple attached to the substrate holder. The system was operated in the temperatures range of 25–950°C and the nitrogen (oxygen) partial pressures range of background pressure (5×10^{-6} Torr at 780°C) to 0.5 Torr to optimize the deposition conditions for various films investigated in this study.

The dc-sputtered TiO_2 films were prepared by a homemade sputtering system [19]. A 50-mm-diameter (99.99% pure) titanium disk was used as the target. The distance between the target and

substrate was about 25 mm. The sputtering was carried out in a 29:1 argon/oxygen mixture at a total pressure of 0.2 Torr. Since the substrates were not intentionally heated during deposition, the as-deposited films were amorphous. TiO_2 films of 20–50 nm thickness were deposited at a typical deposition rate of 0.1 nm/min using a total dc input power of 30 W.

The electrical property of the TiN and YBCO films was measured using the four-probe method. The crystalline structure of the films was examined by X-ray diffraction (XRD, Rigaku D/max-rc/ru200b) using CuKα radiation. The surface morphology of the films was investigated by means of atomic force microscopy (AFM, Digital Instruments DI 5000) and scanning electron microscopy (SEM). The electronic structure of the TiO_2 films prepared by PLD and by dc sputtering techniques was examined by XAS, using the 6 m high-energy spherical monochromatic (HSGM) beam line at Synchrotron Radiation Research Center (SRRC), Taiwan, ROC [20].

3. Results and discussion

3.1. Pulsed laser deposition of TiN films on $SrTiO_3$

The TiN films were prepared with a laser energy density of 5 J/cm^2 and a repetition rate of 5 Hz. The deposition rate under the laser conditions was about 0.02 nm/pulse. The target was a hot-pressed TiN (99.9% pure) pellet. The blue plume could be easily observed during ablation. We have investigated the crystallinity and electrical property of the films obtained under various deposition conditions. It was found that with the above laser operating conditions, the best TiN films were obtained under the background pressure ($\sim 5 \times 10^{-6}$ Torr) and at $T_s = 700$°C. The as-deposited films, typically about 30–80 nm thick, were shiny golden yellow in appearance. Fig. 1(a) shows the XRD pattern of an 80-nm-thick TiN thin film, indicating that the TiN film has grown with a predominance of (1 0 0) texture. The full width at half-maximum (FWHM) of the TiN(2 0 0) θ–2θ diffraction peak was about 0.18°. The surface morphology as revealed by AFM (Fig. 1(b)), shows an average grain size of about 50 nm with a rather smooth surface. The root mean square (RMS) roughness of the surface was estimated to be about 0.2 nm. Fig. 1(c) shows the resistivity versus temperature (R–T) curve of the as-deposited TiN thin film on STO. The nearly perfect metallic behavior and the diminishingly small residual resistance below 20 K are indicative of almost impurity-free crystallinity.

3.2. $YBa_2Cu_3O_7$/pulsed laser deposition-TiN/$SrTiO_3$ bilayer structure

With the excellent electrical property and smooth surface described above, the obtained TiN films seem very suitable as a conductive buffer layer for growing YBCO thin films. A bilayer structure was then prepared by depositing TiN and YBCO layers sequentially on the STO substrate. The thicknesses of TiN and YBCO layers were approximately 50 and 200 nm, respectively.

Fig. 2(a) shows the XRD pattern for the YBCO/TiN bilayer structure formed on the STO(1 0 0) substrate. Strong (0 0 l) diffraction peaks of YBCO can be observed, indicating that the YBCO film grew with a c-axis preferred orientation. The YBCO overlayer shows virtually the same transport properties of typical good quality single-layer YBCO films with a zero resistance temperature (T_{co}) of 89 K (Fig. 2(b)).

We also noted that the diffraction peaks of TiN(2 0 0) and (4 0 0) disappeared after YBCO deposition. Nevertheless, new peaks located at about $2\theta = 27.5°$ and 56.5° showed up (Fig. 2(a)). Since the in situ deposition of YBCO films was usually performed in the oxygen ambient at a high temperature, one would have wondered whether any degradation of TiN took place in such an environment. To clarify this speculation, we etched off the top YBCO layer and found that the gold-colored conductive TiN layer was no longer existed. Instead, the original TiN layer has turned into a transparent insulating layer.

In order to identify the resultant product, a 50-nm-thick TiN film was loaded into the experimental chamber and treated at 780°C for 6 min with an oxygen partial pressure of 0.3 Torr to simulate the YBCO film deposition process. Fig. 3(a) shows the XRD results for the oxidized TiN

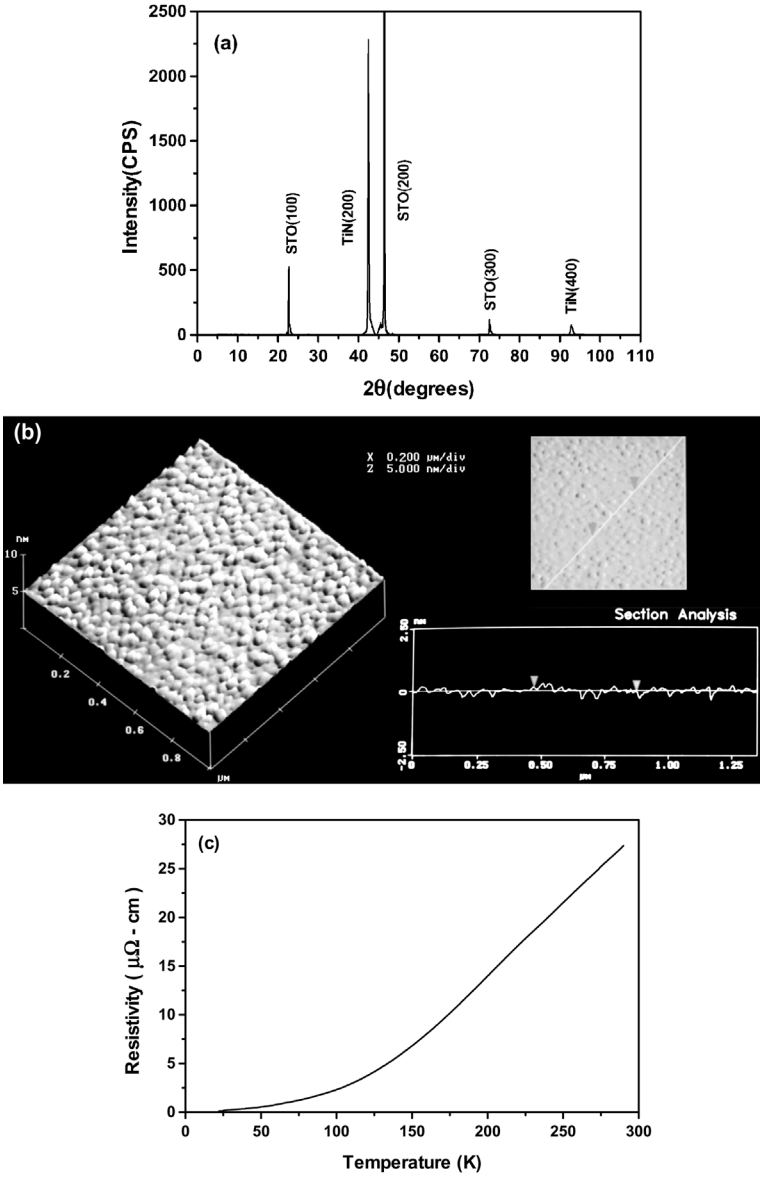

Fig. 1. (a) The X-ray diffraction pattern, (b) the AFM image, and (c) the resistivity versus temperature curve of the TiN(1 0 0) films deposited on STO(1 0 0) substrate. The scanned area of the AFM image was 1×1 μm^2 and the dark-to-light vertical scale was 5 nm.

films. The diffraction peaks, which coincide with those appeared in Fig. 2(a), are identified as that of the rutile TiO_2 with (1 1 0) preferred orientation. This unexpected result suggests that TiN might not be a good underlayer electrode after all, since oxidation seems unavoidable during deposition of YBCO. The AFM image shown in Fig. 3(b) illustrates that the grain size of TiO_2 thus obtained is about 400 nm, which is much larger than that of the original TiN films. A greater variation in roughness (RMS roughness ~ 0.8 nm) can also be observed in the figure.

The thermal oxidation of TiN films has been investigated by many research groups [8,9].

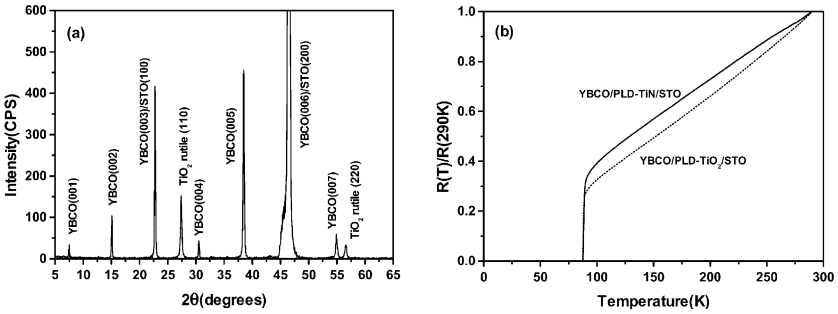

Fig. 2. (a) The X-ray diffraction pattern and (b) the normalized resistance versus temperature curves of the YBCO/PLD-TiN (solid line) bilayer structures formed on the STO(1 0 0) substrate. The dashed line plotted in Fig. 2(b) indicates the *R–T* curve of YBCO/PLD-TiO_2/STO(1 0 0) structure.

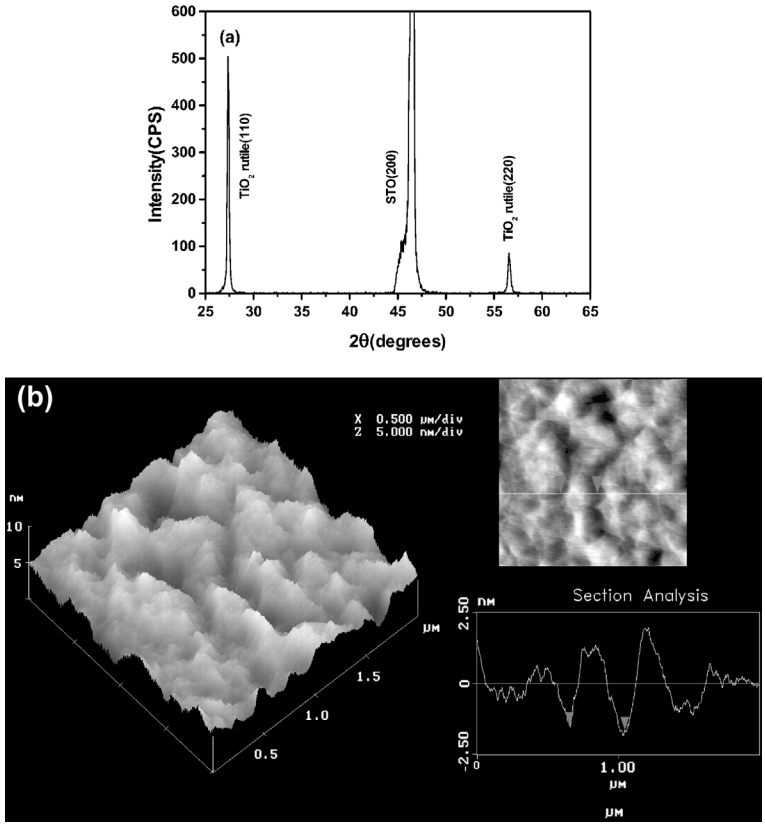

Fig. 3. (a) The X-ray diffraction pattern and (b) the AFM image of the rutile (1 1 0)TiO_2 films oxidized from PLD-TiN films. The scanned area of the AFM image is 2×2 μm^2 and the dark-to-light vertical scale is 5 nm.

Wittmer et al. [8] used Rutherford backscattering spectrometry (RBS) to measure the thickness of the oxidized layer in the temperature range of 500–650°C and observed a parabolic oxidation kinetics described by $d = 2(Dt)^{1/2}$, where d is the thickness of the TiO_2 film, t is the time of oxidation and D is the diffusion coefficient of oxygen in TiO_2. The temperature dependence of D can be written as

$D(T) = D_0 \exp(-E_a/kT)$, where k is Boltzmann's constant, T is the temperature and E_a is the activation energy of the process. Using the values of $E_a = 2.05 \pm 0.05$ eV and $D_0 = 4.3 \times 10^{-2}$ cm^2/s obtained by Wittmer et al [8], we estimate the thickness of TiO_2 films at $T_s = 780$°C can reach 400 nm in 1 min. This is much thicker than the thickness of deposited TiN layer. Therefore, we conclude that TiN(1 0 0) may have transformed into rutile TiO_2(1 1 0) completely prior to the deposition of YBCO films.

3.3. Pulsed laser deposition of TiO_2 films and $YBa_2Cu_3O_7$/pulsed laser deposition-TiO_2/$SrTiO_3$ bilayer structure

Now that the oxidation is unavoidable during deposition of YBCO films, the originally conceived YBCO/TiN bilayer structure should be YBCO/TiO_2 bilayer structure instead. Then we tried to prepare the TiO_2 film by PLD of TiO_2 target directly. In order to reduce particulates on the films during PLD, a 10-mm-diameter rutile TiO_2(1 1 0) single crystal substrate was used as the target. The laser conditions for depositing TiO_2 films were the same as those for depositing TiN films (5 J/cm^2 and 5 Hz). But the deposition rate of the TiO_2 films was about 0.05 nm/pulse.

Pure anatase TiO_2 films were obtained for substrate temperatures ranging from 180°C to 980°C (limited by heater) and the oxygen partial pressures ranging from 10^{-4} to 0.5 Torr. The best films (consider the crystallinity and surface morphology) were obtained at $T_s = 800$°C and an oxygen partial pressure of 10^{-2} Torr. Fig. 4(a) shows the typical XRD pattern of a 80-nm-thick TiO_2 thin

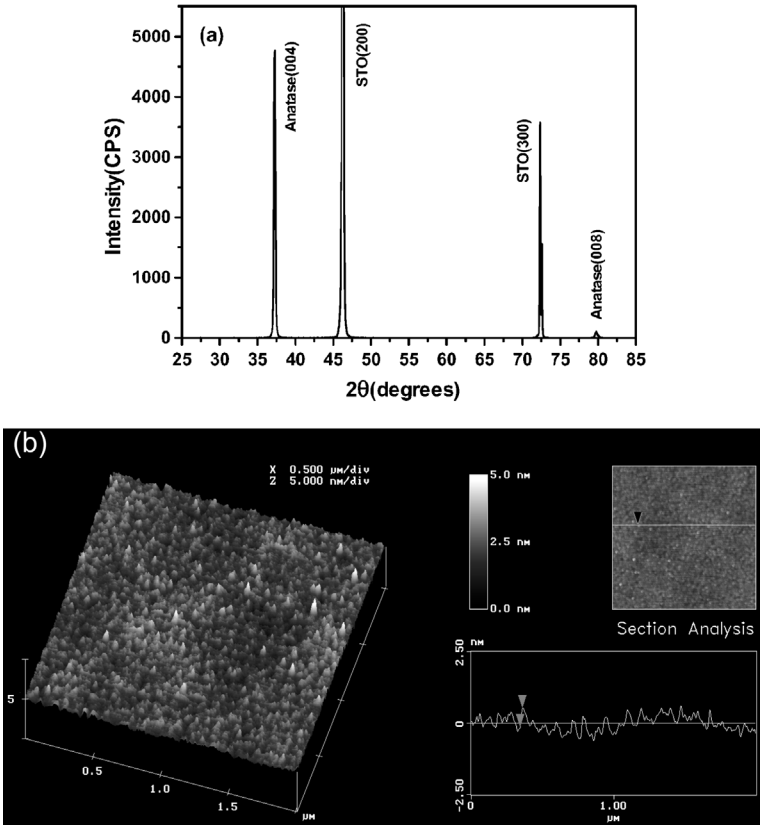

Fig. 4. (a) The XRD pattern and (b) the AFM image of the TiO_2 films prepared by PLD directly. The scanned area of the AFM image is 2×2 μm^2 and the dark-to-light vertical scale is 5 nm.

film deposited at above conditions, indicating that TiO_2 film deposited on STO(1 0 0) substrate was predominantly (0 0 l) oriented anatase phase. The FWHM of the anatase TiO_2(0 0 4) θ–2θ diffraction peak was about 0.19°. The surface morphology (Fig. 4(b)) shows an average grain size of about 50 nm. The RMS roughness of the surface was about 0.25 nm. It seems that, although the phase is different, the surface is very smooth for both PLD-TiN transferred TiO_2 and PLD-TiO_2 films.

As an independent check, both forms of TiO_2 films were further examined by means of XAS measurements. The XAS experiments on the O 1s and Ti 2p spectra were performed on the 6m-HSGM beam line at Synchrotron Radiation Research Center [20]. The spectra were recorded in both total-electron-yield (TEY) mode and X-ray-fluorescence-yield (XFY) mode, which illustrated the surface and bulk properties, respectively [21]. Fig. 5(a)–(e) shows the O 1s spectra for (a) standard rutile TiO_2 powder, (b) standard anatase TiO_2 powder, (c) rutile TiO_2(1 1 0) substrate, (d) TiO_2 films transformed from PLD-TiN films, and (e) direct PLD-TiO_2 films, respectively. In general, the spectra can be roughly divided into two regions [22–24]. The first region covers the energy range 530–537 eV and is attributed to O 2p state hybridized to Ti 3d states. The Ti 3d region is split by crystal field effect and is characterized as a doublet. The second region, above 537 eV, is attributed to O 2p states hybridized to Ti 4sp bands. As shown in Fig. 5, although the peaks lying in the first region has no significant difference between rutile and anatase, there does exist differences in the peaks lying in the second region. At this higher energy region, rutile exhibits three peaks C1, C2 and C3 while anatase shows only two peaks D1 and D2. The intensity variations of these spectra obtained are consistent with those obtained by de Groot et al. [24–26] and evidently indicate that the TiO_2 films are indeed pure anatase or rutile phase.

A bilayer structure by depositing TiO_2 and YBCO layers sequentially on the STO substrate was then prepared. The thicknesses of TiO_2 and YBCO layers were approximately 80 and 200 nm, respectively. The dashed line plotted in Fig. 2(b) shows the normalized resistance versus temperature curve of the YBCO/PLD-TiO_2 bilayer structure. The YBCO film shows the similar transport properties as that of YBCO/PLD-TiN transferred-TiO_2 structure. Therefore, we conclude that high quality superconducting YBCO films can be grown on epitaxial TiO_2 buffer layers regardless that they are rutile or anatase.

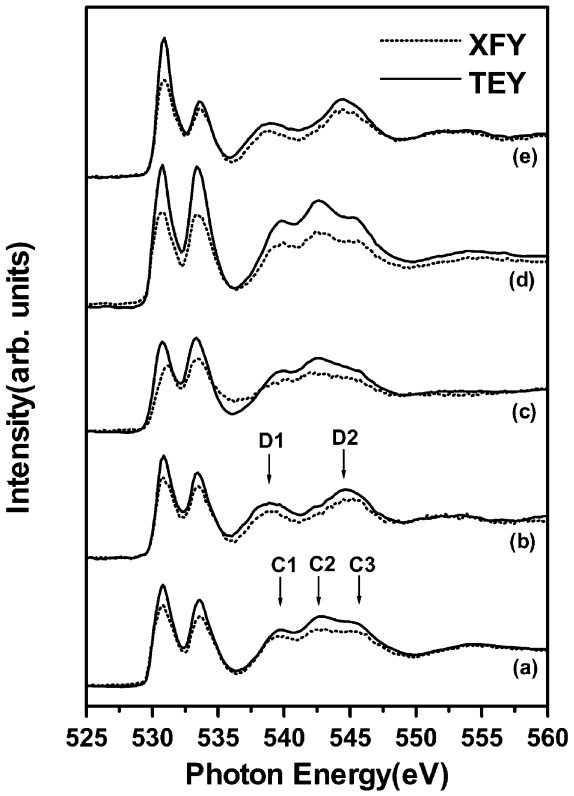

Fig. 5. The XAS spectra of the O 1s spectra for (a) standard rutile TiO_2 powder, (b) standard anatase TiO_2 powder, (c) rutile TiO_2(1 1 0) substrate (used as a target for PLD TiO_2 films), (d) TiO_2 films transformed from PLD TiN films, and (e) direct PLD-TiO_2 films. TEY mode is plotted as a solid line and the XFY mode is plotted as a dashed line.

3.4. TiO_2 films prepared by DC sputtering and selective epitaxial growth technique

As has been described in Section 2, the as-deposited TiO_2 films prepared by dc sputtering were amorphous (as shown in Fig. 6(a)) since the substrates were not intentionally heated during deposition. In order to simulate the changes of

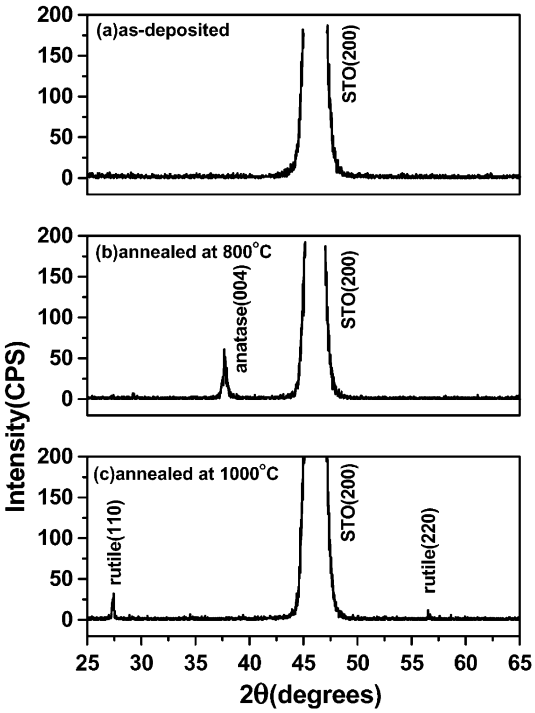

Fig. 6. The XRD pattern of the dc sputtered TiO_2 films. (a) As-deposited film, (b) annealed at 800°C for 6 min, (c) annealed at 1000°C for 6 min.

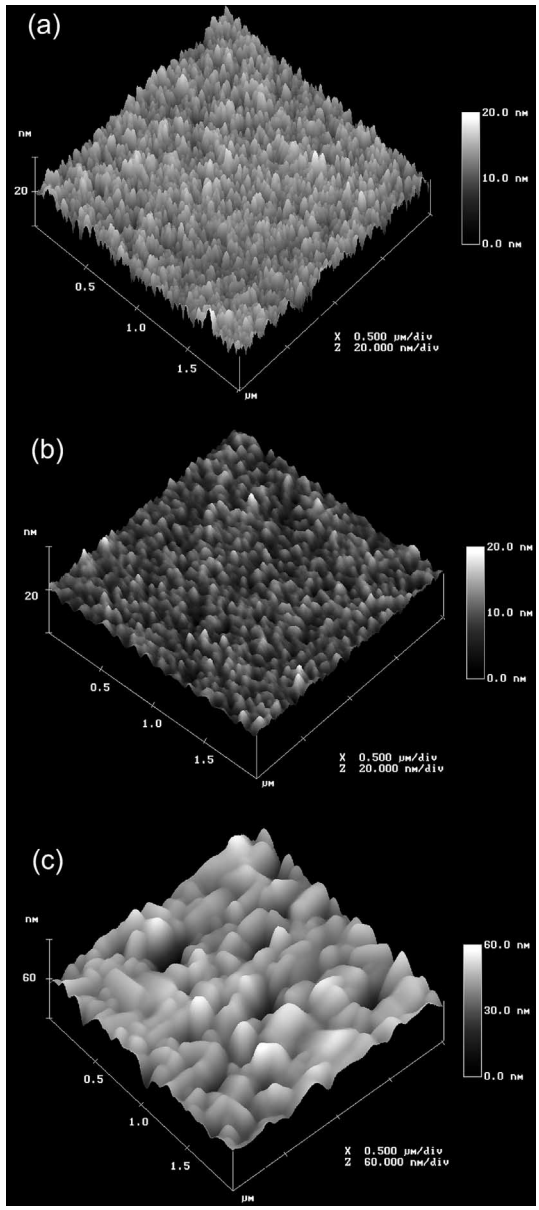

Fig. 7. The AFM images of the dc sputtered TiO_2 films. (a) As-deposited film, (b) annealed at 800°C, (c) annealed at 1000°C. The scanned area of the AFM images is 2×2 μm^2 and the dark-to-light vertical scales are 20 nm for (a) and (b) and 60 nm for (c).

amorphous TiO_2 films prior to YBCO deposition, as-deposited sputtered-TiO_2 films were loaded into a vacuum chamber and annealed at different temperatures ranging from 780°C to 1000°C with a 0.3 Torr oxygen pressure for 6 min. The influences of the heat treatment on the crystallinity and the surface morphology were then investigated. The results of XRD pattern shows that most films annealed at 800°C have turned into an anatase phase (Fig. 6(b)) whereas those annealed at 1000°C have turned into a rutile phase (Fig. 6(c)). However, the relatively weak diffraction intensity and broad FWHM (>0.5°) of these films suggest that the crystallinity of these annealed sputtered-TiO_2 film may not be as good as that of PLD-TiO_2 films. Moreover, the AFM images shown in Fig. 7(a)–(c) further reveal that the surface morphology of the films change distinctly as the temperature rises. The as-deposited films and films annealed at 800°C (anatase TiO_2) are made up of small boulders whereas films annealed at 1000°C (rutile TiO_2) consist of many larger crystals with irregular facets. The average grain sizes of the anatase and

rutile TiO_2 films were about 30 and 100 nm, respectively. The RMS roughness of these films was about 3–10 nm as compared to less than 0.5 nm for the PLD-TiO_2 films.

The procedure for obtaining SEG has been described in previous reports [15,16]. The as-deposited TiO_2 film on STO is patterned using a standard lift-off method. Then YBCO films are deposited by PLD on the pre-patterned substrate. Fig. 8 shows the typical AFM picture of YBCO films prepared by the SEG technique. Smooth, black, and good superconducting properties were obtained for YBCO films grown on the STO substrate directly (right side of the figure), whereas rough, nearly transparent, insulating YBCO films (typical resistivity at room temperature $> 10^5$ Ω cm) with large particulates were obtained for YBCO films grown on TiO_2 buffer layers (left side of the figure). For the latter structure, the absence of an YBCO diffraction peak in XRD measurement indicates that the material is amorphous. The large particulates with dimensions of 200–500 nm were mostly CuO outgrowths, as confirmed by the energy-dispersive X-ray (EDX) analysis [16].

3.5. Comparison the characteristics of $YBa_2Cu_3O_7$/TiO_2/$SrTiO_3$ prepared by different techniques

It is then interesting to distinguish the differences between the TiO_2 films prepared by dc sputtering and PLD methods. It is known that the growth of epitaxial YBCO films is closely related to the initial stages of deposition as nucleation and growth first occur on the substrate. As the deposition proceeds, the formation and evolution of dislocations and other defects start to play more prominent roles [27]. Therefore, the structural properties and the surface morphology of the substrates can influence the final quality of the deposited films drastically. Comparing the XRD and AFM results shown in Figs. 3, 4 and 6, it seems likely that the poor crystallinity and much higher RMS roughness of the annealed sputtered TiO_2 films might be responsible for quenching the superconductivity of the YBCO films grown on it.

Alternatively, subtle and previously unidentified interface layer formed during YBCO deposition might also be possible. In order to examine this speculation, the top-layer YBCO films were etched off to investigate the XAS spectra near the

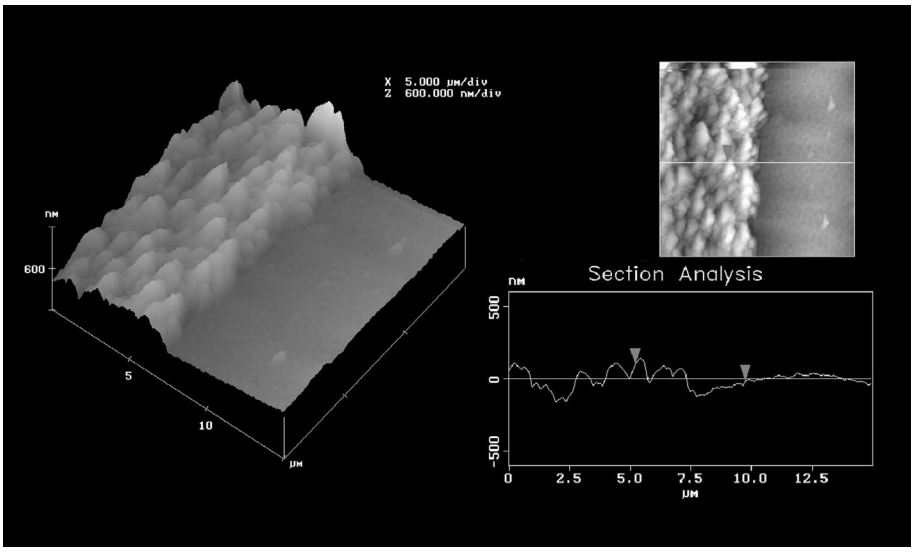

Fig. 8. The AFM image of the YBCO films deposited on STO substrate directly (right side of the figure) and deposited on sputtered-TiO_2 buffer layer (left side of the figure). The TiO_2 films were prepared by dc sputtering. The scanned area of the AFM image is 15×15 μm^2 and the dark-to-light vertical scale is 600 nm.

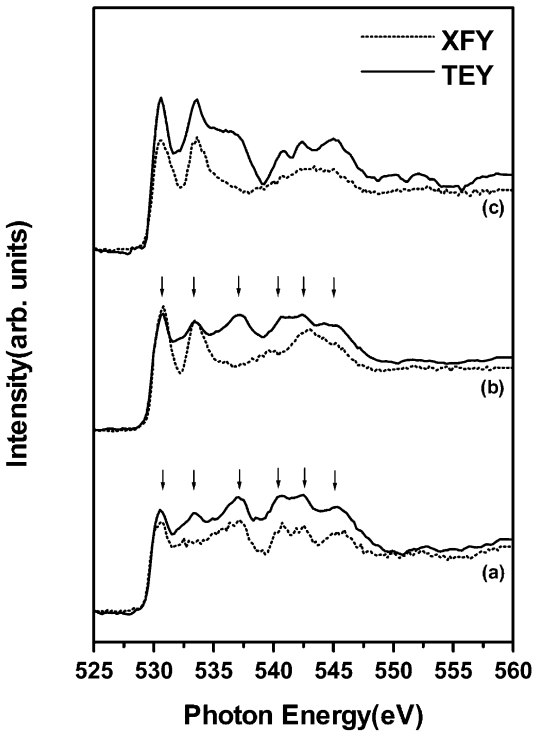

Fig. 9. The XAS spectra of the O 1s spectra for (a) standard $BaTiO_3$ powder, (b) YBCO/PLD-TiN transferred-TiO_2/STO structure and (c) YBCO/dc sputtered-TiO_2/STO structure. The top-layered YBCO films were etched off to investigate the interface between YBCO and TiO_2 films.

interface between YBCO and TiO_2 films. Fig. 9 shows the O 1s spectra for (a) standard $BaTiO_3$ powder, (b) YBCO/PLD-TiN transferred-TiO_2/STO structure and (c) YBCO/dc-sputtered-TiO_2/STO structure (with YBCO removed). It is noted that there exist significant differences in spectral distribution between the XFY mode (bulk properties, plotted in solid line) and the TEY mode (surface characteristics, plotted in dashed line) for the different bilayer structures. As shown in Fig. 9(b) and (c), the XFY results reveal that the TiO_2 films prepared by PLD and dc sputtering are rutile phase. However, the TEY results show that there exists an intermediate layer, which exhibits extremely different characteristics against the TiO_2, between the YBCO and TiO_2 films. The TEY spectrum of the interface between YBCO and PLD-TiN transferred-TiO_2 is very similar to that of $BaTiO_3$ (Fig. 9(a)). However, the TEY spectrum of the interface between YBCO and dc sputtered-TiO_2 cannot match a simple reference spectrum which corresponds to a well-known compound.

In this scenario, during the YBCO growth, the TiO_2 film reacts with the YBCO. A crystalline $BaTiO_3$ layer formed immediately after the first arrival of deposit for YBCO grown on PLD-TiN transferred-TiO_2 (or direct PLD-TiO_2) films. On the other hand, an amorphous Ba–Ti–O compound formed during YBCO grown on sputtered-TiO_2 films. The subsequent YBCO can grow epitaxially on the top of the crystalline $BaTiO_3$ layer [28] and show the superconducting characteristics whereas YBCO cannot grow epitaxially on top of the amorphous Ba–Ti–O compound and, hence, become nonsuperconducting.

4. Summary

TiN and TiO_2 thin films grown on the STO(1 0 0) substrate by PLD are demonstrated to be suitable templates for growing YBCO films. However, although the TiN films originally possessed excellent electrical properties, these failed to serve as the underlayer electrode in an YBCO/TiN/STO bilayer structure since it was readily transformed to rutile(1 1 0) TiO_2 films during the deposition of top-layer YBCO films. For the TiO_2 films deposited on STO(1 0 0) substrate directly, pure anatase TiO_2(0 0 l) films were formed even a pure rutile TiO_2(1 1 0) substrate was used as a target.

In contrast to the good superconductivity obtained in the YBCO/PLD-TiN transferred TiO_2 (or PLD-TiO_2)/STO structure, YBCO films grown directly on a TiO_2 layer prepared by dc sputtering, turned out to be insulating. The surface morphology of TiO_2 films and electronic structure of interfacial layer between YBCO and TiO_2 films have been investigated by AFM and XAS measurements. The results suggest that poor crystallinity and a drastic increase in RMS roughness of the annealed sputtered TiO_2 films *might* have direct influences on growing epitaxial interface like $BaTiO_3$, and thus have influences on growing stoichiometric YBCO films.

Acknowledgements

This work was supported by the National Science Council of Taiwan, ROC under grants: NSC89-2112-M-009-027 and -029.

References

[1] E.I. Meletis, W.B. Carter, R.F. Hochman, Microstr. Sci. 13 (1984) 417.
[2] A. Kohlase, M. Mandl, W. Palmere, J. Appl. Phys. 65 (1989) 2464.
[3] A.J. Silvestre, O. Conde, R. Vilar, M. Jeandin, J. Mat. Sci. 29 (1994) 404.
[4] M. Kiuchi, A. Chayahara, Appl. Phys. Lett. 64 (8) (1994) 1048.
[5] M. Kawamura, Y. Abe, K. Sasaki, J. Vac. Sci. Technol. A 16 (1) (1998) 200.
[6] A. Kumart, J. Narayan, Supercond. Sci. Technol. 6 (1993) 662.
[7] P. Tiwari, T. Zheleva, J. Narayan, Mat. Res. Soc. Symp. Proc. 285 (1993) 311.
[8] M. Wittmer, J. Noser, H. Melchior, J. Appl. Phys. 52 (11) (1981) 6659.
[9] W. Cheung, H. Von Seefeld, M.A. Nicolet, F. Ho, P. Iles, J. Appl. Phys. 52 (1981) 4297.
[10] H.G. Tompkins, J. Appl. Phys. 70 (7) (1991) 3876.
[11] K. Hinode, Y. Homma, M. Horiuchi, T. Takahashi, J. Vac. Sci. Technol. A 15 (4) (1997) 2017.
[12] C. Garapon, C. Champeaux, J. Mugnier, G. Panczer, P. Marchet, A. Catherinot, B. Jacquier, Appl. Surf. Sci. 96–98 (1996) 836.
[13] H. Funakoshi, K. Fumato, M. Okuyama, Y. Hamakawa, Jpn. J. Appl. Phys. 33 (1994) 5262.
[14] J.H. Kim, S. Lee, H.S. Im, Appl. Surf. Sci. 151 (1999) 6.
[15] C.A.J. Damen, H.-J.H. Smilde, D.H.A. Blank, H. Rogalla, Supercond. Sci. Technol. 11 (1998) 437.
[16] Y.K. Cheng, J.T. Lin, Y.C. Chuang, W.C. Huang, S.P. Chen, J.Y. Juang, K.H. Wu. T.M. Uen, Y.S. Gou, Proc. 1999 Int. Workshop Superconductivity, Kauai, Hawaii, ISTEC and MRS, 1999, p. 84.
[17] Y.C. Chuang, J.Y. Juang, K.H. Wu. T.M. Uen, Y.S. Gou, unpublished.
[18] K.H. Wu, J.Y. Juang, C.L. Lee, T.C. Lai, T.M. Uen, Y.S. Gou, S.L. Tu, S.J. Yang, S.E. Hsu, Physica C 195 (1992) 241.
[19] H.L. Chang, C. Wang, M.L. Chu, T.M. Uen, Y.S. Gou, Jpn. J. Appl. Phys. 28 (1989) L631.
[20] S.C. Chung, C.I. Chen, P.C. Tseng, H.F. Lin, T.E. Dann, Y.F. Song, L.R. Huang, C.C. Chen, J.M. Chuang, K.L. Tsang, C.N. Chang, Rev. Sci. Instrum. 66 (1995) 1655.
[21] J. Stohr, NEXASFS Spectrocopy, Springer Series in Surface Sciences 25, Springer, Berlin, Heidelberg, 1992.
[22] J. Pflüger, J. Fink, W. Weber, K.P. Bohnen, H. Winter, Solid State Commun. 44 (1982) 489.
[23] L. Soriano, M. Abbate, J.C. Fuggle, P. Prieto, C. Jiménez, J.M. Sanz, L. Galán, S. Hofmann, J. Vac. Sci. Technol. A 11 (1) (1993) 47.
[24] F.M.F. de Groot, M. Grioni, J.C. Fuggle, J. Ghijsen, G.A. Sawatsky, H. Petersen, Phys. Rev. B 40 (1989) 5715.
[25] F.M.F. de Groot, J.C. Fuggle, B.T. Thole, G.A. Sawatsky, Phys. Rev. B 41 (1990) 928.
[26] R. Brydson, H. Sauer, W. Engel, J.M. Thomas, E. Zeitler, N. Kosugi, H. Kuroda, J. Phys. Condens. Matter. 1 (1989) 797.
[27] K.H. Wu, S.P. Chen, J.Y. Juang, T.M. Uen, Y.S. Gou, Physica C 289 (1997) 230.
[28] S. Hontsu, J. Ishii, H. Tabata, T. Kawai, Appl. Phys. Lett. 67 (1995) 554.